AIP Journal of Applied Physics

Vacancy-type defects in Mg-doped GaN grown by ammonia-based molecular beam epitaxy probed using a monoenergetic positron beam

Akira Uedono, Marco Malinverni, Denis Martin, Hironori Okumura, Shoji Ishibashi, and Nicolas Grandjean

Citation: Journal of Applied Physics **119**, 245702 (2016); doi: 10.1063/1.4954288
View online: http://dx.doi.org/10.1063/1.4954288
View Table of Contents: http://scitation.aip.org/content/aip/journal/jap/119/24?ver=pdfcov
Published by the AIP Publishing

Articles you may be interested in

Proton irradiation effects on deep level states in Mg-doped p-type GaN grown by ammonia-based molecular beam epitaxy
Appl. Phys. Lett. **106**, 022104 (2015); 10.1063/1.4905783

Vacancy-type defects in In x Ga1− x N grown on GaN templates probed using monoenergetic positron beams
J. Appl. Phys. **114**, 184504 (2013); 10.1063/1.4830033

Vacancy-type defects in In x Ga1–x N alloys probed using a monoenergetic positron beam
J. Appl. Phys. **112**, 014507 (2012); 10.1063/1.4732141

Vacancy-type defects in Mg-doped InN probed by means of positron annihilation
J. Appl. Phys. **105**, 054507 (2009); 10.1063/1.3075907

Vacancy-type defects in Er-doped GaN studied by a monoenergetic positron beam
J. Appl. Phys. **103**, 104505 (2008); 10.1063/1.2932166

Reuse of AIP Publishing content is subject to the terms at: https://publishing.aip.org/authors/rights-and-permissions. Download to IP: 130.158.56.92 On: Mon, 22 Aug 2016 01:32:12

JOURNAL OF APPLIED PHYSICS **119**, 245702 (2016)

Vacancy-type defects in Mg-doped GaN grown by ammonia-based molecular beam epitaxy probed using a monoenergetic positron beam

Akira Uedono,[1] Marco Malinverni,[2] Denis Martin,[2] Hironori Okumura,[1,2] Shoji Ishibashi,[3] and Nicolas Grandjean[2]

[1]*Division of Applied Physics, Faculty of Pure and Applied Science, University of Tsukuba, Tsukuba, Ibaraki 305-8573, Japan*
[2]*Institute of Physics, Ecole Polytechnique Fédérale de Lausanne, CH-1015 Lausanne, Switzerland*
[3]*Research Center for Computational Design of Advanced Functional Materials (CD-FMat), National Institute of Advanced Industrial Science and Technology (AIST), Tsukuba, Ibaraki 305-8568, Japan*

(Received 9 March 2016; accepted 8 June 2016; published online 22 June 2016)

Vacancy-type defects in Mg-doped GaN were probed using a monoenergetic positron beam. GaN films with a thickness of 0.5–0.7 μm were grown on GaN/sapphire templates using ammonia-based molecular beam epitaxy and characterized by measuring Doppler broadening spectra. Although no vacancies were detected in samples with a Mg concentration [Mg] below $7 \times 10^{19}\,cm^{-3}$, vacancy-type defects were introduced starting at above [Mg] $= 1 \times 10^{20}\,cm^{-3}$. The major defect species was identified as a complex between Ga vacancy (V_{Ga}) and multiple nitrogen vacancies (V_Ns). The introduction of vacancy complexes was found to correlate with a decrease in the net acceptor concentration, suggesting that the defect introduction is closely related to the carrier compensation. We also investigated Mg-doped GaN layers grown using In as the surfactant. The formation of vacancy complexes was suppressed in the subsurface region ($\leq$80 nm). The observed depth distribution of defects was attributed to the thermal instability of the defects, which resulted in the introduction of vacancy complexes during the deposition process. *Published by AIP Publishing.*
[http://dx.doi.org/10.1063/1.4954288]

I. INTRODUCTION

Gallium nitride (GaN) is widely used to fabricate optoelectronic devices emitting in the blue and near-ultraviolet wavelength ranges,[1] and GaN-based electronic devices have been studied for use in high-power, high-frequency operations.[2] The potential of GaN devices is mainly attributable to the physical properties of GaN, such as its wide bandgap (3.4 eV), large breakdown electric field (3.3 MV cm^{-1}), and high saturation electron velocity ($\sim 2.5 \times 10^7\,cm\,s^{-1}$). Up to now, most GaN-based devices have been fabricated on non-native substrates such as sapphire and SiC using metalorganic vapor phase epitaxy (MOVPE) and molecular beam epitaxy (MBE). Recently, native substrates have started to gain popularity due to advancements in hydride vapor phase epitaxy (HVPE) and ammonothermal GaN growths.[1,3] Substrates produced by those methods are expected to further expand commercialization of optical and electrical devices.

In the fabrication process of GaN devices, controlled impurity doping is essential; Mg is a dopant that enables the reproducible growing of *p*-type GaN. For MOVPE-grown GaN, Mg is doped using a biscyclopentadienyl-magnesium (Cp_2Mg) source, and thermal annealing ($\geq$600 °C) is performed to eliminate hydrogen passivated Mg and activate the dopants.[1,4] MBE has also been successfully used for the growth of *p*-type GaN. Using a solid Mg source, it is possible to grow Mg-doped GaN without hydrogen passivation, and *p*-type GaN with high hole concentrations can be grown without post-growth thermal treatment.[5–7] Because of the large ionization energy of Mg (about 180 meV), however, the hole concentration is only a few percent of the Mg concentration [Mg].[1,8] Thus, one of the main obstacles remaining in the development of high performance GaN devices is the difficulty in achieving high hole concentration.

It is commonly understood that the doping efficiency starts to decrease above [Mg] $\cong 2\times10^{19}\,cm^{-3}$,[9] an effect that has been attributed to the introduction of compensating defects such as point defects, structural defects, Mg precipitates, and polarity inversion domains.[10–13] It has been reported that the use of ammonia-based MBE (NH_3-MBE) coupled with relatively low growth temperatures (740–760 °C) yields the highest hole concentrations.[14,15] In addition, the MBE-growth with an indium surfactant was reported to be effective to suppress the introduction of compensating defect in Mg-doped GaN.[16]

For MBE, low growth temperature should result in lower thermal stress during cooling, less diffusion, and a reduced concentration of compensating centers. However, because MBE film growth is primarily governed by atomic kinetics at the surface, the GaN layers could grow under a non-thermal equilibrium condition, which could introduce defects through post-growth processes. It has also been suggested that the creation of Mg-H complexes during the growth of MOVPE-GaN suppresses the formation of other compensating defects.[10] Thus, knowledge regarding native defects introduced by high Mg doping in MBE-GaN is crucial to improving the optical and electrical properties of GaN-based devices. Positron annihilation, a powerful technique for evaluating vacancy-type defects in semiconductors,[17,18] has been used to investigate defects in group-III nitrides.[19–26] In the present study, we used a monoenergetic positron beam to probe native vacancies in Mg-doped GaN grown by NH_3-based MBE.

Reuse of AIP Publishing content is subject to the terms at: https://publishing.aip.org/authors/rights-and-permissions. Download to IP: 130.158.56.92 On: Mon, 22 Aug 2016 01:32:12

II. EXPERIMENT

In the experiments described in this study, samples of Mg-doped GaN films were grown by NH_3-MBE on the GaN/sapphire templates while varying the Mg concentration between 3×10^{17} and $4 \times 10^{20}\,cm^{-3}$. The specific growth method, morphology, and electrical properties of samples prepared using this method are described elsewhere.[14,27] Si-doped (0001) GaN(4 μm)/sapphire templates were prepared using MOVPE, and they were used as templates. Using NH_3-MBE, after deposition of a 0.5-μm-thick undoped GaN buffer layer on the templates, Mg-doped GaN layers were grown. The thicknesses of the Mg-doped layers were 0.6 μm for the sample with $[Mg] = 3 \times 10^{18}\,cm^{-3}$, 0.7 μm for the sample with $[Mg] = 1.8 \times 10^{19}\,cm^{-3}$, and 0.5 μm for the samples with $[Mg] \geq 4 \times 10^{19}\,cm^{-3}$. The substrate temperature was monitored using an optical pyrometer and kept at 740 °C during growth. Mg was supplied using a RIBER VCOR 100 valved cell, with the concentration [Mg] controlled through the cell temperature and valve opening. The values of [Mg] were estimated using a Mg beam equivalent pressure (BEP). The GaN growth rate was about 400 nm/h at a Ga BEP of 1–4×10^{-5} Pa and a NH_3 flow rate of 200 sccm. All samples were grown under NH_3-rich conditions. The samples with $[Mg] = 4 \times 10^{19}$ and $1 \times 10^{20}\,cm^{-3}$ had indium (In) supplied to the surface during growth to examine the surfactant effect on vacancy-type defects in the Mg-doped GaN layer. The indium BEP was kept at 8×10^{-6} Pa.

Electro-chemical capacitance-voltage (C-V) measurements were performed to determine the net acceptor concentration (N_A–N_D); these were taken well below the surface to avoid parasitic effects related to Mg surface segregation and surface contamination. Impurity concentrations in the substrate were measured by means of secondary ion mass spectrometry (SIMS), and it was shown that the major impurities were hydrogen ($10^{19}\,cm^{-3}$), carbon ($10^{18}\,cm^{-3}$) and oxygen ($10^{18}\,cm^{-3}$). For the sample grown using the surfactant ($[Mg] = 10^{20}\,cm^{-3}$), the In concentration in the Mg-doped GaN layer was $5 \times 10^{17}\,cm^{-3}$. For $In_xGa_{1-x}N$ ($x = 0.05$–0.56), it was reported that the vacancy-type defects were introduced by increasing InN mole fraction,[28] but this effect should not be dominant for the present sample. To serve as a reference sample, 0.6-μm-thick Mg-doped GaN layers were deposited by MOVPE on the GaN/templates and, they were characterized with same experimental conditions. For these samples, the Mg concentration was varied from 3×10^{17} to $5 \times 10^{19}\,cm^{-3}$; their growth method and properties are described elsewhere.[9] For the sake of comparison, a high-quality Si-doped GaN (carrier concentration $= 10^{18}\,cm^{-3}$) grown by HVPE was used. The growth method and properties of the samples prepared by a similar condition which used in the present experiment are described elsewhere.[29]

Details of the positron annihilation technique are described elsewhere.[17,18] In the present experiments, Doppler broadening spectra of the annihilation radiation as a function of the incident positron energy E were measured using Ge detectors. The total counts of the Doppler broadening spectrum were 6×10^5, and the energy resolution of the Ge detector was 1.2 keV (at full width at half maximum: FWHM). The spectra were characterized by the S parameter, defined as the fraction of annihilation events over the energy range of 510.2–511.8 keV, and by the W parameter, defined as the fraction of annihilation events in the ranges of 504.2–507.6 keV and 514.4–517.8 keV. They were also measured using a coincidence system. The total count of the coincidence Doppler broadening spectrum was 3×10^6. The relationship between S and E was analyzed using VEPFIT, a computer program developed by van Veen *et al.*[30] (its application to GaN is described elsewhere[20,31]). The S–E curve was fitted using $S(E) = S_eF_e(E) + S_sF_s(E) + \Sigma S_iF_i(E)$, where $F_e(E)$ is the fraction of non-thermalized (epithermal) positrons annihilated at the surface, and $F_s(E)$ and $F_i(E)$ are the fractions of thermalized positrons annihilated at the surface and in the i-th layer, respectively ($F_e(E) + F_s(E) + \Sigma F_i(E) = 1$). S_e, S_s, and S_b are S parameters, respectively, corresponding to the annihilation of epithermal positrons at the surface and of thermalized positrons at the surface and in the bulk.

Doppler broadening spectra corresponding to the annihilation of positrons were theoretically calculated using QMAS (Quantum MAterials Simulator) code,[32] which uses valence-electron wavefunctions determined by the projector augmented-wave (PAW) method.[33] To describe the exchange and correlation energy of electrons, the generalized gradient approximation was used. Calculations were performed on orthorhombic supercells equivalent to $4 \times 4 \times 2$ wurtzite cells. The supercell dimensions were $2\sqrt{3}a_0 \times 4a_0 \times 2c_0$, where $a_0 = 0.3189$ nm and $c_0 = 1.03725$ nm were the lattice parameters of the wurtzite cell. For the supercell containing a defect, atomic positions in the fixed cell were computationally optimized through a series of first-principles electronic-structure calculations. The formalism of the local density approximation was used in the calculation of the positron wave functions. The simulated spectra were characterized by the S and W parameters, where the energy resolution of the Ge detector was convoluted. The Doppler broadening spectra for the typical cation vacancies were calculated and the results were reported in the previous works.[31,34] The localization of positrons near Mg atom at the N site (Mg_{Ga}) was also reported in Ref. 34. The present paper reports the result of the simulation for $(Mg_{Ga})_2$.

III. RESULTS AND DISCUSSION

A. Behavior of positrons in Mg-doped GaN

Figure 1 displays the S values of Mg-doped GaN grown by NH_3-MBE as a function of incident positron energy E. The S–E curve for HVPE-GaN is also shown. The mean implantation depth of positrons $\bar{z}$ is shown on the upper horizontal axis, where the relationship between $\bar{z}$ and E was given in Ref. 35. For HVPE-GaN, the S value increased with decreasing E, which corresponds to the diffusion of positrons toward the surface: the large S values at low E ($\cong$0.1 keV) are associated with the annihilation of positrons at the surface.[17] The S value saturated at $E > 20$ keV, suggesting that almost all positrons annihilate in the bulk in this energy range. The observed S–E curve was fitted using VEPFIT; the solid curve is a fit to the experimental data. The diffusion length of positrons was obtained as 92 ± 3 nm, a typical

Reuse of AIP Publishing content is subject to the terms at: https://publishing.aip.org/authors/rights-and-permissions. Download to IP: 130.158.56.92 On: Mon, 22 Aug 2016 01:32:12

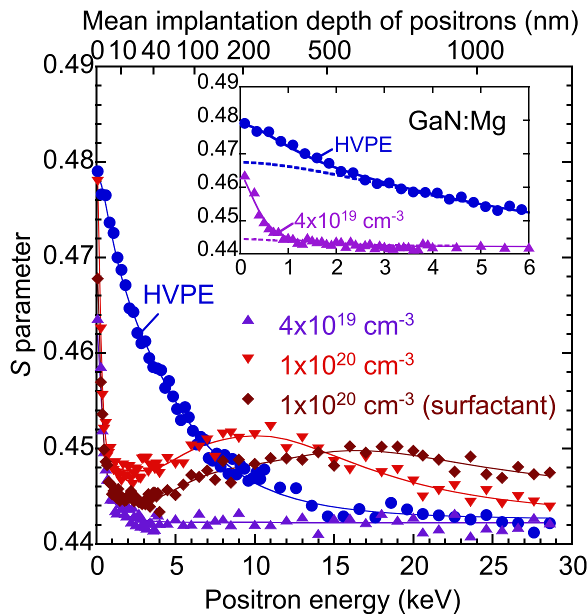

FIG. 1. S parameters as a function of incident positron energy E for Mg-doped GaN grown using NH_3-based MBE with and without an In surfactant. The Mg concentrations are shown in the figure. The solid curves are fits to the experimental data. The result for HVPE-GaN is also shown for the sake of comparison. The inset shows a close up of the S–E curves; the dotted curves are the fitting curves excluding the effect of epithermal positrons on S.

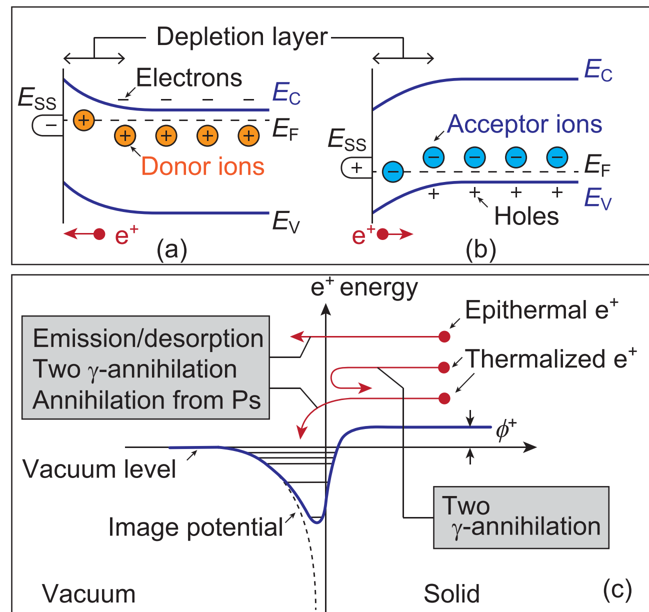

FIG. 2. Schematic diagrams showing the energy levels and charge distributions in (a) n-type and (b) p-type semiconductors, where E_{SS}, E_C, E_V, and E_F are the energy levels of the surface state, the conduction band minimum, the valence band maximum, and the Fermi level, respectively. The drift diffusion of a positron in the depletion region occurs towards the surface in n-type semiconductors, but its direction is opposite for p-type semiconductors (shown as arrows). The diffusion and annihilation behaviors of positrons near the surface are shown in (c). The potential of a thermalized positron is also shown in the same figure.

value for defect-free (DF) GaN, and the S value in the high-energy region (0.442) corresponds to the S value for positron annihilation from the delocalized state.[34,36]

For Mg-doped GaN with $[\mathrm{Mg}] = 4 \times 10^{19}\,\mathrm{cm}^{-3}$, the S values quickly decreased with increasing E. The obtained diffusion length of positrons was 14 ± 5 nm; this short diffusion length indicates the suppression of thermalized positrons diffusing toward the surface. Figures 2(a) and 2(b) schematically show typical surface band bending of n- and p-type semiconductors. It is generally accepted that upward band bending occurs because of the presence of electron traps at the surface of an n-type semiconductor [Fig. 2(a)], causing a decrease in the electron concentration near the surface. This charge distribution introduces an electric field toward the surface in the depletion layer. For a p-type semiconductor [Fig. 2(b)], hole traps at the surface cause downward band bending. Thus, in Mg-doped GaN, the diffusion of positrons toward the surface is suppressed by the electric field introduced by downward band bending.

For HVPE-GaN, the derived value of S_s was 0.4667 ± 0.0004. The dotted lines in the inset of Fig. 1 show the fitting curves excluding the effect of epithermal positrons on S, and the intersection between the dotted line and the vertical axes matches S_s. The S_s value for MBE-GaN with $[\mathrm{Mg}] = 4 \times 10^{19}\,\mathrm{cm}^{-3}$ was derived as 0.4440 ± 0.0004. The observed increase in S at $E \cong 0$ keV for this sample was mainly due to the annihilation of epithermal positrons at the surface. Because of the high kinetic energy of epithermal positrons, its annihilation characteristic is unlikely to be influenced by material properties. The observed behavior of S for p-type GaN has previously been reported,[34,36] and the decrease in the S_s values can be attributed to the annihilation behavior of positrons at the surface of p-type GaN.

Figure 2(c) shows an interaction mechanism for thermalized and epithermal (non-thermal) positrons diffusing back to the surface.[17] Because the positron work function ϕ_+ is negative (2.4 eV),[37,38] thermalized positrons can be emitted to the surface from the bulk. Some positrons are emitted into the vacuum without annihilation; others may annihilate from multiple states, including annihilation with electrons at the surface or annihilation from positronium (Ps: a hydrogen-like bound state between a positron and an electron).[17] Ps exhibits two spin states: para-Ps (p-Ps), a singlet state; and ortho-Ps (o-Ps), a triplet state. P-Ps annihilates via the 2-γ process and emits γ-rays with an energy of 511 keV. Thus, the S value is sensitive to the formation probability of Ps at the surface. No Ps is formed in bulk GaN. Prior to annihilation or Ps formation, positrons might be trapped in the surface image potential or in surface defects. For GaN, the branching ratio has been reported to be 48% positron emission, 12% Ps formation, and 40% annihilation at the surface.[38] For semiconductors, the lifetime of positrons at the surface is longer than the lifetime for bulk annihilation.[17] Using an analogy of the trapping of positrons by vacancy-type defects, the S value corresponding to the positron-electron annihilation at the surface is considered to be higher than that corresponding to bulk annihilation. Thus, the p-Ps annihilation and the positron-electron annihilation at the surface are the origins of the large S value at the surface. For p-type GaN, however, it can be assumed that the positron wave function at the surface is pushed back toward the bulk because of the presence of holes at the surface [Fig. 2(b)], which suppresses the positron-electron annihilation and/or

Reuse of AIP Publishing content is subject to the terms at: https://publishing.aip.org/authors/rights-and-permissions. Download to IP: 130.158.56.92 On: Mon, 22 Aug 2016 01:32:12

the Ps annihilation at the surface. As a result, the S_s value decreases at the surface of Mg-doped GaN.

In *p*-type GaN, Mg acts as a shallow trapping center for positrons, and the localization of the positron wave function around Mg near the surface also could suppress positron annihilation at the surface. It has been reported that the positron density increases near Mg, suggesting that Mg_{Ga} acts as a shallow trap for positrons.[34] Calculations showed that a further localization occurs for $(Mg_{Ga})_2$. Doppler broadening spectra obtained for Mg_{Ga} and $(Mg_{Ga})_2$ were characterized in terms of *S* and *W* parameters, which turned out to be close to those for defect-free (DF) GaN (Fig. 4). Therefore, we can conclude that no large change in *S* and *W* occurs when positron localization occurs around Mg_{Ga} or $(Mg_{Ga})_2$. However, because these act as trapping centers, positron diffusion toward the surface is suppressed. The behavior of positrons near Mg_{Ga} might be analogous to hole localization or hydrogen trapping by Mg_{Ga}.[10,39]

B. Vacancy-type defects introduced by Mg doping to GaN

As shown in Fig. 1, the *S* values at $E > 1$ keV for the sample with $[Mg] = 1 \times 10^{20}\,cm^{-3}$ were higher than those for the sample with $[Mg] = 4 \times 10^{19}\,cm^{-3}$, suggesting the introduction of vacancy-type defects Mg doping. The obtained *S*–*E* curve for the sample without the surfactant was analyzed using four layers in the fitting model. The Mg-doped layer was divided into two layers (first and second layers), and third and fourth layers correspond to the undoped GaN layers grown by MBE and MOVPE, respectively. The *S*–*E* curve was well reproduced without assuming the positron annihilation at the interfaces between those layers. The *S* values for the first and second blocks (S_1 and S_2) were found to be 0.4476 ± 0.0002 and 0.4520 ± 0.0004, respectively. The position of the interface between the first and second layers, $D_{1/2}$, was found to be 70 ± 10 nm. The same analysis was performed for the sample with the surfactant, and the values of S_1, S_2, and $D_{1/2}$ were obtained to be 0.4446 ± 0.0002, 0.4488 ± 0.0004, and 80 ± 10 nm, respectively. From these analyses, it can be concluded that the introduction of vacancies was suppressed in the subsurface region ($\leq$80 nm); we will discuss the depth profiles of vacancies in Mg-doped layers later. For the sample with the surfactant ($[Mg] = 10^{20}\,cm^{-3}$), the *S* values at $E > 18$ keV were higher than those for the sample without the surfactant, which can be attributed to the high *S* value corresponding to the annihilation of positrons in the undoped GaN layer. For this sample, oxygen was found to accumulate at the interface between undoped GaN layers grown by MBE and MOVPE, and its concentration at the interface was $8 \times 10^{19}\,cm^{-3}$. This phenomenon was observed only in this sample. No penetration of In was observed below the undoped MBE-GaN layer. Thus, the introduction of defects in the undoped MBE-GaN layer might be related to unintentionally incorporated oxygen at the surface of the template (contamination), and a resultant degradation of the crystal quality of the undoped MBE-GaN layer.

Figure 3 shows the values of N_A–N_D and *S* averaged using the values measured at $E = 6$–8 keV as a function of [Mg]. As shown in Fig. 3(b), the *S* values for the sample with $[Mg] < 10^{20}\,cm^{-3}$ were almost identical to the *S* value for HVPE-GaN, suggesting that no detectable defects were introduced by Mg doping. This result also applies to the sample grown by MOVPE. The *S* values began to increase above $[Mg] = 10^{20}\,cm^{-3}$, although the increase was suppressed in the sample grown with the surfactant. In Fig. 3(a), the value of N_A–N_D increases with increasing [Mg] but begin to decrease above $[Mg] = 10^{20}\,cm^{-3}$. This can be associated with the introduction of carrier compensation centers owing to the over-doping of Mg. The detailed relationships between Mg BEP, [Mg], N_A–N_D, and hole mobility have previously been reported for Mg-doped GaN prepared using a method similar to that used in the present work,[40] and the same trends observed. In this study, the highest N_A–N_D value

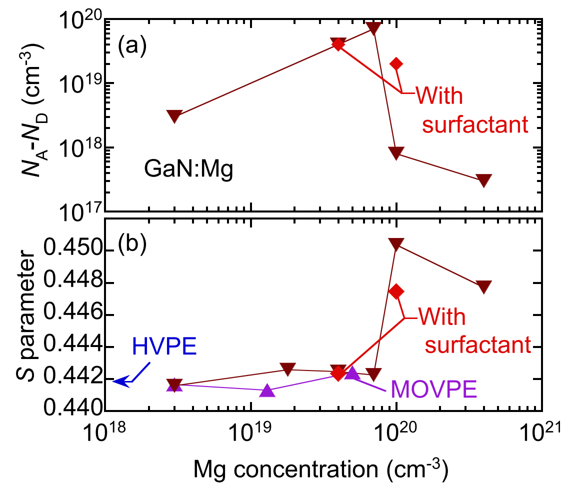

FIG. 3. (a) Net acceptor concentration (N_A–N_D) and (b) the averaged values of *S* measured at $E = 6$–8 keV for Mg-doped GaN grown by MBE and MOVPE as a function of Mg concentration.

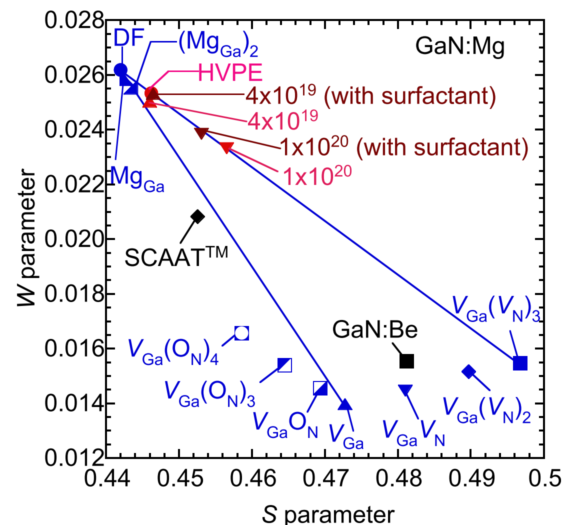

FIG. 4. *S*–*W* relationships for Mg-doped MBE-GaN grown with and without an In surfactant. The Mg concentrations are shown in the figure. The value of *E* was fixed at 7 keV. The result for HVPE-GaN is also shown ($E = 30$ keV). The (*S*,*W*) values were calculated using the QMAS code for positron annihilation in defect-free (DF), $V_{Ga}V_N$, $V_{Ga}(V_N)_n$, $V_{Ga}(O_N)_n$ (n = 1–4), Mg_{Ga}, and $(Mg_{Ga})_2$. The (*S*,*W*) values for Be-implanted GaN (GaN:Be)[20] and bulk GaN grown by an ammonothermal method (SCAAT)[41] are also shown.

Reuse of AIP Publishing content is subject to the terms at: https://publishing.aip.org/authors/rights-and-permissions. Download to IP: 130.158.56.92 On: Mon, 22 Aug 2016 01:32:12

obtained was $7 \times 10^{19}\,\mathrm{cm}^{-3}$, which agrees well with the value of [Mg] measured by SIMS. At $[\mathrm{Mg}] = 10^{20}\,\mathrm{cm}^{-3}$, the N_A–N_D value for the sample grown with the surfactant was higher than that for the sample without the surfactant. We attribute this to the suppression of the introduction of compensation centers by the surfactant. From the observed relationship between S and N_A–N_D, it can be concluded that the V_{Ga}-related defects closely correlate with the introduction of the carrier compensation centers.

Figure 4 shows the S–W relationships for Mg-doped GaN grown with and without In surfactants. These values were obtained from the coincidence Doppler broadening spectra measured at $E = 7$ keV ($\bar{z} = 120$ nm), where the positrons implanted with this energy mainly annihilate in the first and second layers in Mg-doped GaN which used in the fitting procedure. A result for HVPE-GaN in which the value of E was fixed at 30 keV is also shown. This (S,W) value is used as the reference for the positron annihilation from the delocalized state. The statistical error bars of the (S,W) values were close to the size of symbol used in the figure. The QMAS code was used to simulate typical V_{Ga}-type defects [$V_{Ga}(V_N)_n$, $V_{Ga}(O_N)_n$, n = 1–4], Mg_{Ga}, $(Mg_{Ga})_2$, and the (S,W) values for the annihilation of positrons in the delocalized state (DF), as shown in Fig. 4. The difference between the calculated (S,W) values for DF-GaN and those for HVPE-GaN (which lie to the lower right of the DF-GaN values in the figure) could have a variety of causes, including limitations on the first-principles calculations applied to Doppler broadening spectra, the effects of the experimental background, and/or the energy resolution of the Ge detectors. In a sample containing vacancy-type defects, positrons can annihilate from delocalized and trapped states; in such cases, the (S,W) value is obtained as a weighted average of the characteristic (S,W) values for those states, and the (S,W) value should lie on a line connecting these values. The (S,W) values for the samples with $[\mathrm{Mg}] = 4 \times 10^{19}\,\mathrm{cm}^{-3}$ were almost identical to that for HVPE-GaN, suggesting that no detectable defects were present in these samples.

In Fig. 4, the (S,W) values for Be-implanted GaN[20] and bulk GaN grown by an ammonothermal method[41] are also shown. For Be-implanted GaN (shown as GaN:Be), the (S,W) value corresponds to the positron annihilation in the damaged region introduced by ion implantation. Because the nearest neighbor of the (S,W) value for GaN:Be is the value for a divacancy ($V_{Ga}V_N$), the major defect species was identified as $V_{Ga}V_N$. The bulk GaN was grown by the ammonothermal method in supercritical ammonia using an acidic mineralizer. The result of this sample is referred as SCAAT^{TM}. The major impurities were oxygen and hydrogen, and their concentrations were around $8 \times 10^{17}\,\mathrm{cm}^{-3}$. The (S,W) values for GaN grown by SCAAT are found on the left-hand side of the line connecting the calculated values for DF and V_{Ga}, suggesting that the major defect species in GaN grown by SCAAT is not "pure" V_{Ga} or $V_{Ga}(V_N)_n$, but vacancy-impurity complexes. Thus, the major defect species was identified as a Ga vacancy coupled with impurities such as oxygen.

The (S,W) value for the sample with $[\mathrm{Mg}] = 1 \times 10^{20}\,\mathrm{cm}^{-3}$ (grown without the surfactant) was found on the line connecting the calculated values for DF and $V_{Ga}(V_N)_3$ (in the figure, the line connecting the values for DF and $V_{Ga}(V_N)_3$ is shown). Although the one of the major impurities is oxygen, the (S,W) values for the $V_{Ga}(O_N)_n$ (n = 1, 3, 4) are far from the value for this sample. Thus, the major defect species can be identified as V_{Ga} coupled with multiple V_Ns. V_N has been suggested as one of the major carrier compensation centers of Mg-doped GaN.[10] Some of V_N preferentially couple with V_{Ga} and can form stable complexes.[42] We can therefore conclude that the observed behavior of defects in the $[\mathrm{Mg}] = 1 \times 10^{20}\,\mathrm{cm}^{-3}$ sample is attributable to the introduction of V_N and the related formation of $V_{Ga}V_N$ complexes. In Fig. 3, the S value for the sample with $[\mathrm{Mg}] = 4 \times 10^{20}\,\mathrm{cm}^{-3}$ is smaller than that for the sample with $[\mathrm{Mg}] = 1 \times 10^{20}\,\mathrm{cm}^{-3}$. This phenomenon can be attributed to positron localization near Mg nanoclusters and either a resulting suppression of positron trapping by $V_{Ga}V_N$ complexes, or a transform and collapse of vacancy complexes into larger three-dimensional defects such as stacking faults. In the latter case, positrons could annihilate in the open spaces adjacent to such defects. For the samples at the highest Mg concentration, a positron might annihilate inside such clusters. The (S,W) value for DF metallic Mg was calculated by the QMAS code, and was obtained to be (0.607, 0.0108). The calculated S value is larger than the S values measured for the present samples. Therefore, assuming that the crystal structure of metallic Mg is similar to that of the nanoclusters, the observed decrease in the S value for Mg-doped GaN cannot be explained by the localization of positrons in the nanoclusters.

As shown in Fig. 1, the S values at $E = 2$–4 keV were almost constant for the samples with $[\mathrm{Mg}] = 1 \times 10^{20}\,\mathrm{cm}^{-3}$ grown using the surfactant, and they increased above $E = 4$ keV. Thus, the formation of the defect complexes in the subsurface region was suppressed in the samples with high [Mg], a tendency that was accelerated when surfactant was used. The introduction of defects in the deeper area would occur during film growth, which suggests that the formation of the vacancy complexes depends not only on [Mg] but also on the deposition processes such as a growth and post-deposition cooling speeds.

IV. SUMMARY

We used positron annihilation spectroscopy to study vacancy-type defects in Mg-doped GaN grown by NH_3-MBE. Doppler broadening spectra were measured using a monoenergetic positron beam as a function of the incident energy of positrons E. Coincidence Doppler broadening spectra were measured to identify the defect species. The depth distributions of vacancy-type defects were determined from the S–E curves. For the sample with $[\mathrm{Mg}] \leq 7 \times 10^{19}\,\mathrm{cm}^{-3}$, no detectable vacancies were introduced. Above $[\mathrm{Mg}] = 1 \times 10^{20}\,\mathrm{cm}^{-3}$, vacancy-type defects started to appear, with the major defect species that was identified as a complex between V_{Ga} and multiple V_Ns. The introduction of these defect complexes was accompanied by a decrease in N_A–N_D, suggesting that the carrier compensation in Mg-doped GaN is closely related to the formation of the vacancy complexes. For the sample with $[\mathrm{Mg}] = 1 \times 10^{20}\,\mathrm{cm}^{-3}$, the introduction of vacancy complexes

Reuse of AIP Publishing content is subject to the terms at: https://publishing.aip.org/authors/rights-and-permissions. Download to IP: 130.158.56.92 On: Mon, 22 Aug 2016 01:32:12

was suppressed through the use of an In surfactant during film growth, with the value of N_A–N_D increasing as a result. The observed inhomogeneity of the defect distribution could be attributed to the thermal instability of defects during or after film growth. We have shown that the positron annihilation parameters are sensitive to native vacancy-type defects in Mg-doped GaN, and that positron annihilation spectroscopy is a useful tool for optimizing the growth parameters of Mg-doped GaN.

ACKNOWLEDGMENTS

One of the authors (A.U.) would like to thank Professor Y. Nanishi (Ritsumeikan University) for his valuable discussions.

[1]*Introduction to Nitride Semiconductor Blue Lasers and Light-Emitting Diodes*, edited by S. Nakamura and S. F. Chichibu (Taylor and Francis, London, 2000).
[2]B. J. Baliga, Semicond. Sci. Technol. **28**, 074011 (2013).
[3]R. Dwiliński, R. Doradziński, J. Garczyński, L. Sierzputowski, R. Kucharski, M. Zając, M. Rudziński, R. Kudrawiec, J. Serafińczuk, and W. Strupiński, J. Cryst. Growth **312**, 2499 (2010).
[4]S. Nakamura, T. Mukai, and M. Senoh, Appl. Phys. Lett. **64**, 1687 (1994).
[5]W. Kim, A. E. Botchkarev, A. Salvador, G. Popovici, H. Tang, and H. Morkoç, J. Appl. Phys. **82**, 219 (1997).
[6]M. Hansen, L. F. Chen, S. H. Lim, S. P. DenBaars, and J. S. Speck, Appl. Phys. Lett. **80**, 2469 (2002).
[7]W. Fong, C. Zhu, B. Leung, C. Surya, B. Sundaravel, E. Luo, J. Xu, and I. Wilson, Microelectron. Reliab. **42**, 1179 (2002).
[8]W. Götz, R. S. Kern, C. H. Chen, H. Liu, D. A. Steigerwald, and R. M. Fletcher, Mater. Sci. Eng. B **59**, 211 (1999).
[9]A. Castiglia, J.-F. Carlin, and N. Grandjean, Appl. Phys. Lett. **98**, 213505 (2011).
[10]C. G. Van de Walle and J. Neugebauer, J. Appl. Phys. **95**, 3851 (2004).
[11]P. Vennéguès, M. Benaissa, B. Beaumont, E. Feltin, P. De Mierry, S. Dalmasso, M. Leroux, and P. Gibart, Appl. Phys. Lett. **77**, 880 (2000).
[12]I. P. Smorchkova, E. Haus, B. Heying, P. Kozodoy, P. Fini, J. P. Ibbetson, S. Keller, S. P. DenBaars, J. S. Speck, and U. K. Mishra, Appl. Phys. Lett. **76**, 718 (2000).
[13]N. Grandjean, B. Damilano, and J. Massies, J. Phys.: Condens. Matter **13**, 6945 (2001).
[14]A. Dussaigne, B. Damilano, J. Brault, J. Massies, E. Feltin, and N. Grandjean, J. Appl. Phys. **103**, 013110 (2008).
[15]C. Hurni, J. Lang, P. Burke, and J. Speck, Appl. Phys. Lett. **101**, 102106 (2012).
[16]E. C. H. Kyle, S. W. Kaun, E. C. Young, and J. S. Speck, Appl. Phys. Lett. **106**, 222103 (2015).
[17]R. Krause-Rehberg and H. S. Leipner, *Positron Annihilation in Semiconductors, Solid-State Sciences* (Springer-Verlag, Berlin, 1999), Vol. 127.
[18]F. Tuomisto and I. Makkonen, Rev. Mod. Phys. **85**, 1583 (2013).
[19]K. Saarinen, T. Suski, I. Grzegory, and D. C. Look, Phys. B: Condens. Matter **308–310**, 77 (2001).
[20]A. Uedono, K. Ito, H. Nakamori, K. Mori, Y. Nakano, T. Kachi, S. Ishibashi, T. Ohdaira, and R. Suzuki, J. Appl. Phys. **102**, 084505 (2007).
[21]O. Moutanabbir, R. Scholz, S. Senz, U. Gösele, M. Chicoine, F. Schiettekatte, F. Süßkraut, and R. Krause-Rehberg, Appl. Phys. Lett. **93**, 031916 (2008).
[22]M. J. Wang, L. Yuan, C. C. Cheng, C. D. Beling, and K. J. Chen, Appl. Phys. Lett. **94**, 061910 (2009).
[23]S. Hautakangas, J. Oila, M. Alatalo, and K. Saarinen, Phys. Rev. Lett. **90**, 137402 (2003).
[24]S. Hautakangas, K. Saarinen, L. Liszkay, J. A. Freitas, Jr., and R. L. Henry, Phys. Rev. B **72**, 165303 (2005).
[25]J. Xu, Q. Li, W. Zhang, J. Liu, H. Du, and B. Ye, Chem. Phys. Lett. **616–617**, 161 (2014).
[26]X. F. Li, Z. Q. Chen, C. Liu, H. J. Zhang, and A. Kawasuso, J. Appl. Phys. **117**, 085706 (2015).
[27]M. Malinverni, J.-M. Lamy, D. Martin, E. Feltin, J. Dorsaz, A. Castiglia, M. Rossetti, M. Duelk, C. Vélez, and N. Grandjean, Appl. Phys. Lett. **105**, 241103 (2014).
[28]A. Uedono, S. Ishibashi, T. Watanabe, X. Q. Wang, S. T. Liu, G. Chen, L. W. Sang, M. Sumiya, and B. Shen, J. Appl. Phys. **112**, 014507 (2012).
[29]K. Fujito, S. Kubo, H. Nagaoka, T. Mochizuki, H. Namita, and S. Nagao, J. Cryst. Growth **311**, 3011 (2009).
[30]A. van Veen, H. Schut, M. Clement, J. M. M. de Nijs, A. Kruseman, and M. R. IJpma, Appl. Surf. Sci. **85**, 216 (1995).
[31]A. Uedono, S. Ishibashi, N. Oshima, and R. Suzuki, Jpn. J. Appl. Phys., Part 1 **52**, 08JJ02 (2013).
[32]S. Ishibashi, T. Tamura, S. Tanaka, M. Kohyama, and K., Terakura, Phys. Rev. B **76**, 153310 (2007).
[33]P. E. Blöchl, Phys. Rev. B **50**, 17953 (1994).
[34]A. Uedono, S. Takashima, M. Edo, K. Ueno, H. Matsuyama, H. Kudo, H. Naramoto, and S. Ishibashi, Phys. Status Solidi B **252**, 2794–2801 (2015).
[35]J. Gebauer, S. Eichler, R. Krause-Rehberg, and H. P. Zeindl, Appl. Surf. Sci. **116**, 247 (1997).
[36]A. Uedono, S. Ishibashi, K. Tenjinbayashi, T. Tsutsui, K. Nakahara, D. Takamizu, and S. F. Chichibu, J. Appl. Phys. **111**, 014508 (2012).
[37]C. D. Beling, S. Fung, L. Ming, M. Gong, and B. K. Panda, Appl. Surf. Sci. **149**, 253 (1999).
[38]L. V. Jørgensen and H. Schut, Appl. Surf. Sci. **255**, 231 (2008).
[39]J. Buckeridge, C. R. A. Catlow, D. O. Scanlon, T. W. Keal, P. Sherwood, M. Miskufova, A. Walsh, S. M. Woodley, and A. A. Sokol, Phys. Rev. Lett. **114**, 016405 (2015).
[40]H. Okumura, D. Martin, M. Malinverni, and N. Grandjean, Appl. Phys. Lett. **108**, 072102 (2016).
[41]A. Uedono, Y. Tsukada, Y. Mikawa, T. Mochizuki, H. Fujisawa, H. Ikeda, K. Kurihara, K. Fujito, S. Terada, S. Ishibashi, and S. F. Chichibu, J. Cryst. Growth **448**, 117–121 (2016).
[42]X. M. Duan and C. Stampfl, Phys. Rev. B **79**, 174202 (2009).

Reuse of AIP Publishing content is subject to the terms at: https://publishing.aip.org/authors/rights-and-permissions. Download to IP: 130.158.56.92 On: Mon, 22 Aug 2016 01:32:12